Chemosphere 346 (2024) 140635

Contents lists available at ScienceDirect

Chemosphere

journal homepage: www.elsevier.com/locate/chemosphere

Anodic abatement of glyphosate on Pt-doped SnO_2–Sb electrodes promoted by pollutant-dopant electrocatalytic interactions

Raúl Berenguer [a,*], Maribel G. Fernández-Aguirre [a,b], Samuel Beaumont [a], Francisco Huerta [c], Emilia Morallón [a]

[a] Instituto Universitario de Materiales and Departamento de Química Física. Universidad de Alicante, Apartado 99, E-03080, Alicante, Spain
[b] Escuela Profesional de Química, Facultad de Ciencias, Universidad Nacional de Ingeniería, Av. Túpac Amaru, 210, Lima, Peru
[c] Departamento de Ingeniería Textil y Papelera, Universitat Politècnica de València, Pza Ferrándiz y Carbonell, E-03801 Alcoy, Alicante, Spain

HIGHLIGHTS

- Pt nanophases dispersed in SnO_2–Sb electrocatalyze GLP oxidation and mineralization.
- GLP adsorbs on Pt through carboxylate groups to reduce its refractory character.
- Adsorption on Pt synergistically cooperate with oxidizing •OHs produced by SnO_2–Sb.
- Pt-doped SnO_2–Sb anodes can eliminate GLP by consuming half the energy needed by BDD.

GRAPHICAL ABSTRACT

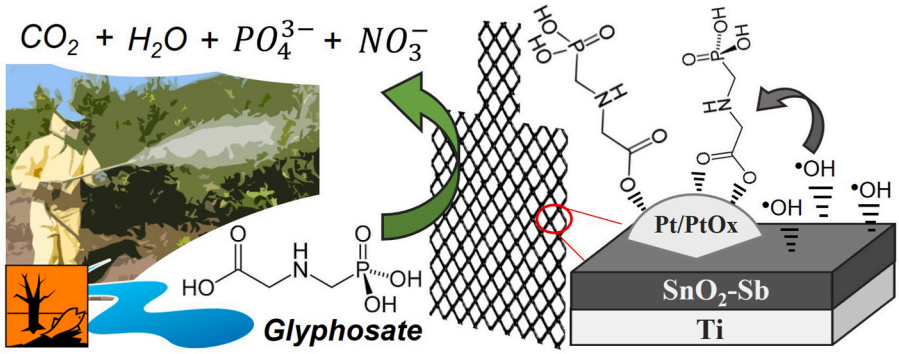

ARTICLE INFO

Handling Editor: E. Brillas

Keywords:
Glyphosate
Anodic oxidation
Tin oxide electrodes
Electrocatalysis
Water treatment

ABSTRACT

The development of non-expensive and efficient technologies for the elimination of Glyphosate (GLP) in water is of great interest for society today. Here we explore novel electrocatalytic effects to boost the anodic oxidation of GLP on Pt-doped (3-13met%) SnO_2–Sb electrodes. The study reveals the formation of well disperse Pt nanophases in SnO_2–Sb that electrocatalyze GLP elimination. Cyclic voltammetry and in-situ spectroelectrochemical FTIR analysis evidence carboxylate-mediated Pt-GLP electrocatalytic interactions to promote oxidation and mineralization of this herbicide. Interestingly, under electrolytic conditions Pt effects are proposed to synergistically cooperate with hydroxyl radicals in GLP oxidation. Furthermore, the formation of by-products has been followed by different techniques, and the studied electrodes are compared to commercial Si/BDD and Ti/Pt anodes and tested for a real GLP commercial product. Results show that, although BDD is the most effective anode, the SnO_2–Sb electrode with a 13 met% Pt can mineralize GLP with lower energy consumption.

* Corresponding author.
E-mail address: raul.berenguer@ua.es (R. Berenguer).

https://doi.org/10.1016/j.chemosphere.2023.140635
Received 14 July 2023; Received in revised form 5 November 2023; Accepted 5 November 2023
Available online 6 November 2023

1. Introduction

Because of their increasing use and disposal, persistence and bioaccumulation, as well as potential toxicological effects, emerging pollutants constitute a group of substances that pose a serious threat to the environment and human health (Deblonde et al., 2011; Geissen et al., 2015). So much so that some of these compounds have been included in the list of priority substances by European Union's commissions (Lamastra et al., 2016).

Among different emergent pollutants present in water, both academia and institutions have a huge interest in the monitoring and control of glyphosate (GLP), the most used herbicide in the world. In 2015 the International Agency for Research on Cancer (IARC) stated that GLP can be carcinogenic to animals and probably to humans (Grosse et al., 2016; Kalofiri et al., 2021; Kissane and Shephard, 2017; World Health Organization, 2017). Moreover, other multiple harmful effects of GLP have been reported (Grosse et al., 2016; Kalofiri et al., 2021; Kissane and Shephard, 2017; Oláh et al., 2022). Despite of these concerns, however, the European Union (EU) renewed the permission to use GLY for an additional year, so it is currently approved until December 15, 2023 and further extension will depend on the ongoing peer review process (European Commission, 2023). This EU position is thus in agreement with the contrary assessments of the European Food Safety Authority (EFSA) and the European Chemicals Agency (ECHA), as well as the US Environmental Protection Agency (US EPA), which have considered GLP as not or unlikely to be carcinogen (Székács and Darvas, 2018). In parallel, while the field of herbicide-tolerant crops is increasing, and even more countries are approving herbicide-tolerance technology for crops, there are not efficient alternatives to GLP (European Commission, 2023). In this sense, the global GLP market is expected to grow with a fast adoption by farmers (ISAAA, 2020). In particular, various market research companies predict GLP market to keep a compound annual growth rate (CAGR) between 6.0 and 7.5 % over this decade (IndustryARC, 2022; Mordor Intelligence, 2022; Transparency Market Research, 2022), in such a case reaching a global market volume of USD 17.7 billion by the end of 2031.

Considering this scenario of GLP, the case surrounding re-registration of this active herbicide ingredient has become one of the most controversial societal issues today regarding emerging pollutants in the EU (European Commission, 2023; Székács and Darvas, 2018). Most importantly, while this global economic, environmental and health debate continues, the development of efficient and sustainable technologies for GLP abatement becomes urgent.

Several strategies have been attempted for the elimination of this pollutant in water. The studied conventional methodologies include adsorption on porous materials (De Santana et al., 2006; Glass, 1987; Morillo et al., 1997; Nourouzi et al., 2010), the use of membranes (Carneiro et al., 2015; Hosseini and Toosi, 2019), as well as biological processes (Zhang et al., 2015) and oxidizing agents (Assalin et al., 2010; Barrett and Mcbride, 2005). On the other hand, based on the generation of highly oxidizing radicals (*e.g.*, hydroxyl radical •OH), advanced oxidation processes (AOPs) have received special attention to perform a partial or total degradation of the pollutant molecules (Wang and Xu, 2012). In the case of GLP, AOPs like H_2O_2/UV (Ikehata and El-Din, 2006; Mariani et al., 2015), Fenton (Ikehata and El-Din, 2006), photo-oxidation (Assalin et al., 2010; Ikehata and El-Din, 2006; Muneer and Boxall, 2008), photo-fenton (De Souza et al., 2013), electro-fenton (Balci et al., 2009) have been investigated. Apart from the discrepancy on degradation efficiencies along this literature, however, there are some important drawbacks on these processes. Thus, the use of expensive consumable materials and/or chemicals that additionally pollute the water, the control of pH for Fenton reactions, or the need of light-dependent devices remarkably hinder the widespread application of these technologies.

Anodic oxidation is probably the simplest AOP (Kapałka et al., 2010; Martínez-Huitle and Ferro, 2006; Panizza and Cerisola, 2009). Basically, this technique is based on the generation of •OH radicals from water over a polarized anode surface, enabling degradation of toxic and/or refractory pollutants and pathogens in water. Interestingly, it operates at ambient conditions (pressure and temperature), without adding or generating other reagents, avoiding pH control and adjustment, and the need of light or other activation systems. Moreover, it avoids the formation of chlorinated by-products present in traditional degradation processes (Kapałka et al., 2010; Martínez-Huitle and Ferro, 2006; Panizza and Cerisola, 2009). However, the efficiency, selectivity and lifetime, as well as the cost and sustainability of this technology relies on the selection of a suitable anode (electrocatalyst) material (Cañizares et al., 2002; Kapałka et al., 2009).

Among several choices, the Boron-Doped Diamond (BDD) and commercial Pt (Ti/Pt) electrodes have been the most studied (Cañizares et al., 2002; Marselli et al., 2003; Panizza et al., 2001; Rodrigo et al., 2001). So far, the "non-active" behavior and matchless capability of BDD to generate highly oxidizing •OH radicals from water make it to exhibit the highest performance towards the anodic abatement of organic compounds. However, important drawbacks remain for the utilization of BDD at industrial scale, being its excessively high cost and fragility the mayor concerns. By contrast, Pt shows a good catalytic activity towards the competitive oxygen evolution reaction (OER) and, therefore, a low current efficiency and capability towards •OH radicals' generation for organics destruction. Then, despite their good stability, the poor performance together with the high cost of Ti/Pt electrodes strongly limit their use for anodic remediation.

Constituted by single or mixed metal oxides supported onto Ti, the extraordinary versatility and stability under OER made the dimensionally stable anodes (DSAs) (Trasatti, 2000) to be considered as the most promising alternatives to the above anodes. Nevertheless, the high cost and good activity for the OER shown for the most stable compositions, based on IrO_2 and RuO_2, have also supposed important barriers for the development of this technology. Then, for years the focus of interest has been mainly aimed to the study of DSAs based on PbO_2 and SnO_2 (Comninellis and Pulgarin, 1993; Polcaro et al., 1999), which are much cheaper and present a high overpotential for the competing OER. Thus, several studies and decades later, the oxidation efficiency of anodes is merely associated to their capability for •OHs generation. This simplified picture of the state of the art may reflect a lack of progress on electrocatalysis in this field. In this sense, exploring novel electrocatalytic effects different to •OHs generation may be relevant not only for this field, but it could also contribute to develop other processes and technologies.

Parallel to the research on anode materials, various studies have been devoted to demonstrate the capability of anodic oxidation towards the abatement of emerging pollutants (Lan et al., 2018; Loos et al., 2018; Montenegro-Ayo et al., 2023; Sirés and Brillas, 2012). However, few studies have been focused on the electroxidation of GLP (Neto and de Andrade, 2009; Kukurina et al., 2014; Rubí-Juárez et al., 2016; Tran et al., 2017). In fact, apart from being a threatening pollutant, the study of the oxidation of this compound deserves great interest because of the particular structure of this compound, which gathers terminal carboxylic and phosphate groups linked by an amine. Considering the potential risks associated to GLP, then, the study of electrocatalysts for GLP oxidation is a hot research topic and a subject of general interest to society.

Focused on electrocatalysis applied to environment, our research group has been working for years on the design and study of non-expensive MOx-like anodes for wastewater treatment (Berenguer et al., 2014, 2016, 2017, 2019a, 2019b; Fernández-Aguirre et al., 2005, 2020; Montilla et al., 2004a, b, c; 2005). It has been demonstrated that the specific pollutant-metal interactions can cause outstanding electrocatalytic effects on the performance of DSA-like anodes, enabling even to overcome the oxidation performance of BDD (Berenguer et al., 2017, 2019a). Thus, current efficiencies of around 100 % were obtained for cyanide electroxidation by doping cobalt spinel with copper, i.e.

extraordinarily by using cheap "active" metal oxides, what was attributed to Cu-cyanide catalytic interactions (Berenguer et al., 2017).

On the other hand, we have studied SnO_2–Sb anodes doped with small amounts of Pt (3–13 met%) for pollutants degradation (Berenguer et al., 2014, 2016, 2019b; Fernández-Aguirre et al., 2005, 2020). Although the main role of Pt was to stabilize SnO_2–Sb (Berenguer et al., 2014; Montilla et al., 2004a), this metal was found to introduce interesting catalytic properties for the oxidation of organics (Berenguer et al., 2016, 2019b; Fernández-Aguirre et al., 2020; Montilla et al., 2005). In fact, we have recently demonstrated that the incorporation of Pt into the SnO_2–Sb coatings enhances the kinetics and efficiency for diclofenac oxidation and mineralization, interestingly, despite hindering the •OHs generation (Fernández-Aguirre et al., 2020). Although the existence of specific interactions of the organic molecules with Pt was hypothesized to electrocatalyze their oxidation (Berenguer et al., 2019b; Fernández-Aguirre et al., 2020), the catalytic effects on these promising anodes are not understood yet.

In this context, the objective of the present work is to study the electrocatalytic behavior of Pt-doped SnO_2–Sb anodes, paying special attention on their potential application for GLP abatement in water. For this purpose, Ti/SnO_2–Sb–Pt (0, 3, 13 met%) anodes were prepared by conventional thermal decomposition. As important novelty, the electrodes were characterized by Field Emission Scanning Electron Microscopy (FE-SEM) to study the presence of nano-sized Pt phases. Then, the electrochemical behavior of GLP on polycrystalline Pt surface was analyzed by cyclic voltammetry (CV) and in-situ FTIR spectroscopy. Next, the effect of Pt-doping on the electrocatalytic response of SnO_2–Sb electrodes towards GLP oxidation was explored by CV and galvanostatic experiments in a filter-press cell. In these experiments, the evolution of GLP concentration, total organic carbon (TOC), chemical oxygen demand (COD), and oxidation by-products was followed as a function of time to get insight into the electroxidative reaction pathways of GLP. Furthermore, the practical application of these anodes was evaluated by comparison with Ti/Pt and BDD commercial anodes and by using not only self-prepared solutions but also commercial GLP (real herbicide product).

2. Experimental

2.1. Chemicals

Glyphosate (N-(phosphonomethyl) glycine) was an analytical standard; tin chloride pentahydrate ($SnCl_4 \cdot 5H_2O$) and hexachloroplatinic acid hexahydrate ($H_2PtCl_6 \cdot 6H_2O$) were from Aldrich; antimony trichloride ($SbCl_3$) was from Fluka; sulfuric acid (H_2SO_4) with an assay of 95%, was from VWR Chemicals; absolute ethanol (EtOH), with an assay of 99.9%, were from J.T. Baker. All chemicals were used as received. Commercial Glyphosate in the form of Glyphosate Isopropylamine Salt, being 36% w/v, was from Belchim. Ultrapure water from a Milli-Q® HX 7000 SD equipment (18.2 MΩ cm) was used for the preparation of the aqueous solutions.

2.2. Anode materials

Antimony tin oxide electrodes were prepared by following a methodology developed by our group in previous works (Berenguer et al., 2014; Montilla et al., 2005). In a brief, a thermal decompositions of salt precursors ($SnCl_4$ •$5H_2O$, $SbCl_3$ and H_2PtCl_6) were carried out in acidified absolute ethanol over a mesh (5 × 4cm) or plate (1 × 1cm) of Ti, provided by INAGASA. The nomenclature of the studied electrodes was established related to the content of platinum (metal atomic composition) being Ti/SnO_2–Sb–Pt (x%), with x = 3 and 13 met% Pt. The commercial Ti/Pt electrode was provided by INAGASA and BDD was provided by Adamant Technologies, supported over a Si plate (Si/BDD). A pre-treatment was performed to all the electrodes, by submitting them to a constant current density of 10 mA cm^{-2} for 5 min to clean and stabilize the surface.

2.3. Physicochemical characterization of the synthesized anodes

The Ti/SnO_2–Sb–Pt (x%) electrodes were analyzed by different techniques. The formation of segregated phases and general morphology, as well as the bulk composition were analyzed by Field Emission Scanning Electron Microscopy and energy dispersive X-ray (EDX) microanalysis, respectively. FE-SEM images were obtained with a Merlin VP Compact microscope (ZEISS) operated at 2 kV, coupled to a Quantax 400 X-ray detector (BRUKER). For EDX-mapping analysis, and trying to maximize the resolution, the electrodes were excited at 5 kV to collect information only of the M-type electron transitions. According to Castaing's formula (Heinrich, 1968), the analytical area (minimum spot) at 5 kV of platinum (21.37 kg m^{-3} density) was 50 nm and above 150 nm for Sn and Sb (150 nm for Sn and 175 nm for Sb).

The microstructure of the electrodes was studied by X-ray diffraction (XRD). For the measurements, a KRISTALLOFLEX K 760−80F diffractometer (Bruker D8-Advance) with a Ni-filtered Cu Kα radiation (λ = 1.5416 Å) was used. Diffraction data points were recorded stepwise within $2\theta = 20-80^\circ$ at a scan rate of 1° min^{-1} with a scan step of 0.05° and a preset time of 3 s. The average crystallite dimensions were calculated from the full width at half maximum (FWHM) of main reflections by using the Scherrer's equation (Klug and Alexander, 1974). The surface chemistry was characterized by X-ray photoelectron spectroscopy (XPS) in a K-Alpha spectrometer (Thermo-Scientific) with Mg Kα radiation (hν = 1253.6 eV). Binding energies were referenced against the main C (1s) line of adventitious carbon impurities at 284.5 eV and given to an accuracy of 0.2 eV. For quantification, nonlinear Shirley background subtraction was applied and peak areas were normalized by using appropriate atomic sensitivity factors.

2.4. In situ FTIR characterization

The electrochemical interaction of Pt with GLP was studied at room temperature by in situ Fourier-transform Infrared reflection absorption spectroscopy (FT-IRRAS), which is one of the most powerful tools to monitor electrode processes (Lozeman et al., 2020). For these experiments, a polycrystalline platinum (Poly-Pt) disc electrode was used as working electrode. On the other hand, the spectroscopic measurements were performed by using a Nicolet 5700 spectrometer, provided with a liquid-nitrogen cooled mercury cadmium telluride (MCT) detector, and assembled to a spectroelectrochemical cell, as previously reported (Iwasita and Nart, 1995). The IR beam traversed a prismatic CaF_2 window, then irradiating the electrode surface at an angle of incidence of 60°. The cell was connected to a Standard Potenciost Wenkin ST 72 and an EG&G PARC mod. 175 signal generator. In this case, a reversible hydrogen electrode (RHE) was the reference electrode and, to avoid the interference of water-derived vibrations, a 0.5 M GLP + 0.1 M H_2SO_4 solution in deuterium oxide was used. During the measurements, the electrode potential was fixed at different values and, then, IR spectra were obtained at a resolution of 8 cm^{-1} after averaging of 200 interferograms. A platinum wire was used as a counter electrode. Prior the experiments, the electrolyte solutions were de-oxygenated by N_2 bubbling and the Poly-Pt electrode was flame-cleaned and rinsed in ultrapure water.

2.5. Electrochemical behavior towards GLP oxidation

The electrochemical properties of the synthesized and commercial electrodes to be used as electrocatalysts for GLP oxidation were studied by cyclic voltammetry. In addition, a Poly-Pt sphere was also used to better study the Pt-GLP interaction. The electrodes were submerged in a three-electrode electrochemical cell containing a 0.5 M H_2SO_4 aqueous solution in N_2 atmosphere in the absence (blank electrolyte) or presence of 200 mg L^{-1} of GLP. The total submerged surface of these working

electrodes was 0.95 cm^2 for Poly-Pt, 1 cm^2 for BDD and 2 cm^2 for the rest of anode materials. Prior the experiments, the electrolyte solutions were de-oxygenated by N_2 bubbling and the Poly-Pt electrode was flame-cleaned and rinsed in ultrapure water. The counter electrode was a Pt wire, and the reference electrode was an Ag/AgCl/Cl^- (3 M KCl) commercial electrode. The voltammetric experiments were carried out by using a VSP Biologic potentiostat (Biologic Science Instruments). A constant scan rate of 50 mV s^{-1} was used through the experimental series.

2.6. Electrolysis of pure and commercial GLP

The performance of the anode materials during the electrochemical degradation of GLP was studied at constant current (1.0 A) in a single compartment filter-press cell. In a typical experiment, 200 mL of a 200 mg L^{-1} GLP in a 0.5 M H_2SO_4 aqueous solution (referred to as pure GLP or self-prepared solution) was continually recirculated at 40.6 mL s^{-1} between the cell and the electrolyte tank, which was temperature-controlled to keep 298 K along the experimental series. A stainless-steel plate (310L) was used as a cathode, and an Ag/AgCl/Cl^-(3 M KCl) reference electrode was connected by a luggin capillary in order to follow the potential of anode materials. The total submerged surface area of studied anodes was 20 cm^2. Thus, a moderate constant current density of 50 mA cm^{-2} was applied for 48 h to the cell, taking electrolyte samples to follow the GLP degradation during time. At this point it is important to stress that these experimental conditions are neither optimized nor intended to reproduce/simulate any wastewater treatment conditions. Instead, the chosen conditions are just suitable to study and compare the electrocatalytic behaviors of the different electrodes under controlled conditions.

The experimental series were repeated by substituting the self-prepared GLP solution with a commercial GLP solution and a treatment time of 30 h. This solution contained an unknown concentration of other unspecified substances, but it was diluted in aqueous 0.5 M H_2SO_4 to 200 mg L^{-1} GLP salt. In any case, the concentration and degradation of GLP was monitored by the growing phosphate concentration during the electrochemical treatment, since GLP ($C_3H_8NO_5P$) total oxidation in aqueous media produces PO_4^{3-} ions as one of the final degradation products, by following Eq. (1). This concentration was followed by a standardized phosphate test method at UV–Vis analyzer Spectroquant Nova 60. The same equipment was used for the determination of chemical oxygen demand (COD) for the commercial GLP experimental series by using standardized COD test to the results obtained for the different electrodes.

$$C_3H_8NO_5P + 8\bullet OH \rightarrow 3CO_2 + PO_4^{3-} + NO_3^- + 16H^+ + 12e^- \quad (1)$$

The state of GLP mineralization was determined by following the evolution of the total organic carbon (TOC) during the experimental series, measured in a TOC-$V_{CSH/CSN}$ Shimadzu equipment. Determination of oxidation by-products, including aminomethylphosphonic acid (AMPA) (which is the main metabolite found in plants due to GLP partial degradation (Mañas et al., 2009)), PO_4^{3-}, organic acids (acetic and formic), and N species (NH_4^+, NO_2^- and NO_3^-), was performed by ionic chromatography (IC), in a DIONEX DX 500 equipment.

Several parameters were then calculated to determine the performance of each electrode.

The *oxidation efficiency (%), OE* (Eq. (2)), related to the global yield of oxidation at each electrode, was calculated from the values of phosphate concentration obtained at the end of the galvanostatic treatment ($[PO_4^{3-}]_f$) respect to the theoretical phosphate concentration ($[PO_4^{3-}]_{0,theo}$) calculated for a total conversion of pure GLP according to Eq. (1).

$$OE = \frac{[PO_4^{3-}]_f}{[PO_4^{3-}]_{0,theo}} \cdot 100 \quad (2)$$

Since the decay of GLP was observed to be exponential, [GLP] data were fitted to a pseudo-first order kinetics (Eq. (3)) to calculate the GLP oxidation rate constant (s^{-1}) , k_1:

$$Ln\frac{[GLP]}{[GLP]_0} = -k_1 \cdot t \quad (3)$$

The *TOC efficiency (%), TE* (Eq. (4)), was used to determine the capability of electrodes to mineralize GLP. This parameter was calculated from the values of TOC obtained at the end of every experiment ($[TOC]_f$) respect to the initial TOC concentration of the GLP solution ($[TOC]_0$).

$$TE = \frac{\left([TOC]_0 - [TOC]_f\right)}{[TOC]_0} \cdot 100 \quad (4)$$

The *current efficiency (%), CE,* for each treatment was calculated from Eq. (5):

$$CE = \left(\frac{nFV(\Delta TOC)_{exp}}{4.32 \cdot 10^7 mIt}\right) \cdot 100 \quad (5)$$

where n is the number of electrons consumed in the mineralization of GLP, which was taken as 12 after complete oxidation and mineralization to CO_2, according to Eq. (1). F is Faraday's constant (96485 C mol^{-1}), V is the solution's volume (L), $(\Delta TOC)_{exp}$ is the experimental TOC decay (mg L^{-1}) evaluated as the difference between the initial value and that analyzed at any electrolysis time t (h), $4.32 \cdot 10^7$ is a conversion factor (3600 s h^{-1} · 12000 mg mol C^{-1}), I is the applied current (A) and m corresponds to the number of carbon atoms present in the GLP molecule (3 C atoms). Please note that in this work the energy efficiency of the electrodes was calculated at identical current densities (instead of identical electrode potentials) because of practical considerations, since these conditions are easier to control in electrolytic experiments (under intense gas bubbling); they are more advantageous to adjust the reaction kinetics; and they better simulate a typical anodic wastewater treatment. On the other hand, the choice of a suitable anode potential for comparative purposes might be controversial, especially when different oxidation mechanisms occur, and in a different extent, depending on this potential (as in the case of glyphosate oxidation on the studied anodes).

Moreover, two additional parameters were calculated for the commercial GLP experimental series. The *COD removal efficiency (%)*, *COD,E* (Eq. (6)), a key parameter for the application of environmental technologies, was derived from the COD obtained at the end of every experiment ($[COD]_f$) respect to the COD of the initial GLP solution ($[COD]_0$):

$$COD,E = \frac{\left([COD]_0 - [COD]_f\right)}{[COD]_0} \cdot 100 \quad (6)$$

Finally, the *energy consumption (kJ L mg^{-1})* to decrease a single TOC unit, U_{TOC}, was determined by following Eq. (7):

$$U_{TOC} = \left(\frac{I\int_{t_0}^{t} Edt}{(\Delta TOC)_{exp} * 1000}\right) \quad (7)$$

where I is the applied current (A), E is the cell voltage (V) (see Table S1 in supporting information, SI) at any time t (s), and $(\Delta TOC)_{exp}$ is the experimental TOC decay (mg L^{-1}), as described above.

3. Results and discussion

3.1. Physicochemical characterization of the electrodes

The main structural and chemical features of the Pt-doped SnO_2–Sb electrodes utilized in this work have been previously studied in detail (Berenguer et al., 2004b, 2004c, 2014). Basically, the electrodes consist

of a 2.2–2.4 μm layer (ca. 1.5–1.7 mg cm^{-2} loadings) of rutile-like SnO_2 cassiterite (from XRD, see the inset of Fig. 1) mixed with Sb and Pt species. XRD and X-ray absorption (EXAFS) measurements evidenced the substitution of Sn^{+4} atoms by Sb^{+5} in the SnO_2 structure, while platinum was proposed to segregate forming dispersed particles in the oxide layer (Socrates, 1994). Morphologically, the coatings exhibit the characteristic cracked-mud surface of DSA-like anodes prepared by thermal decomposition method (see Fig. S1 in SI). The incorporation of Pt lessens the number and dimensions of surface cracks (Fig. 1a), thus contributing to improve the electrochemical stability of Ti/SnO_2–Sb electrodes in different media (Berenguer et al., 2014; Montilla et al., 2004a).

Despite the crucial role of Pt in the electrocatalytic properties these electrodes, however, the formation of platinum phases has not been studied yet. The higher resolution imaging capability of FE-SEM enabled to visualize the fine morphology of the coatings. As observed in Fig. 1b, the surface of Pt-doped Ti/SnO_2–Sb electrodes present a large amount of uniformly dispersed nanoparticles. Specifically for the electrode with 13 met.% Pt, these nanoparticles are less than 35 nm (diameter). The clear brighter contrast of these nanoparticles in the back-scattered electrons image (Fig. 1c) indicates that they correspond to a heavier element in the mixed oxide. Considering the remarkable higher atomic mass of Pt compared to those of Sn and Sb, these nanoparticles are assigned to segregated platinum phases dispersed in the oxide layer.

EDX mapping (see Fig. S2 in SI) confirmed the uniform dispersion of Pt in the oxide coating, but the smaller dimensions of nanoparticles (compared to the spot of EDX microanalysis, minimized to ca. 100 nm) impeded the unequivocal image-composition fitting. Nonetheless, the formation of the platinum-rich phases in the studied electrodes was further confirmed by XRD. Thus, the XRD patterns of the Pt-doped Ti/SnO_2–Sb electrodes (**inset of** Fig. 1) show the peaks corresponding to the (111), (200) and (220) reflections of platinum metallic phase (face centered cubic lattice, JCPDS 04–0802), together with those attributed to the SnO_2-based coating (Cassiterite JCPDS 41–1445) and the underlaying Ti substrate (α-Ti, JCPDS01-089-5009). As observed, the relative intensity of these peaks (i.e., the Pt crystallite dimensions) increases with the Pt percentage in the deposited layer. From Scherrer equation, the mean crystallite size of Pt was calculated to be 10.6 and 11.6 nm for the Ti/SnO_2–Sb electrodes with 3 and 13 met%, respectively.

Finally, XPS was used to analyze the surface chemical composition of the electrodes. The results agree with those previously reported (Montilla et al., 2004c). Briefly, surface Sb was mainly found as Sb^{+5} in a percentage close to the nominal one (ca. 13 met.%) for the electrode without Pt (see Table S2 in SI). However, the incorporation of Pt in the coatings was higher than that expected from the nominal values (6 and 15 met% for the Ti/SnO_2–Sb electrodes with nominal 3 and 13 met%, respectively, see Table S2). The 4f7/2 core-level spectrum of Pt (see Fig. S3 in SI) reveals that this dopant is present with different oxidation states, namely, Pt^0, Pt^{+2} and Pt^{+4}, in both Pt-containing samples.

3.2. Electrochemical interaction of platinum with GLP

The previous characterization has proved the existence of Pt nanophases dispersed in the Pt-doped Ti/SnO_2–Sb electrodes. Then, the electrochemical interaction of platinum with GLP was first studied. For this purpose, a polycrystalline Pt (Poly-Pt) electrode, a pure and well-known electrocatalyst material, was used.

Fig. 2a shows the FTIR spectra registered at different potentials of the Poly-Pt electrode immersed in a H_2SO_4 solution containing 200 mg L^{-1} of GLP. The spectra are presented in the form of normalized differential reflectance referred to a reference spectrum obtained at −0.15 V. Thus, each single spectrum represents changes in vibrational modes occurring at increasing sample potentials relative to the unique reference spectrum at −0.15 V. Three negative bands are clearly observed, being assigned to: (blue line at 1735 cm^{-1}) the stretching of C═O double bonds in carboxylic groups; (red line at 1415 cm^{-1}) the asymmetric stretching mode of O–C–O in carboxylate groups ($-CO_2^-$); and (green line at 1285 cm^{-1}) the stretching of P═O double bonds in phosphate groups (Socrates, 1994). Each band intensity was integrated and plotted as a function of the applied potential, as shown in Fig. 2b. It can be observed that the integrated intensity of the three bands linearly increases with the electrode potential, reaching in all cases a maximum value at a potential close to 1.0 V.

In parallel, the Pt-GLP system was studied by cyclic voltammetry (Fig. 2c). The response of Poly-Pt submerged in the GLP-free electrolyte (dashed line) allows to observe the classical two couples at low potentials assigned to the adsorption (negative scan) and desorption (positive scan) of hydrogen and bisulphate on Pt surface (Konishi et al., 2007). On the other hand, the large reduction current and subsequent oxidation shoulder around −0.20 V are due to the hydrogen evolution reaction. Moreover, the overlapped anodic currents from 0.60 to 1.30 V are

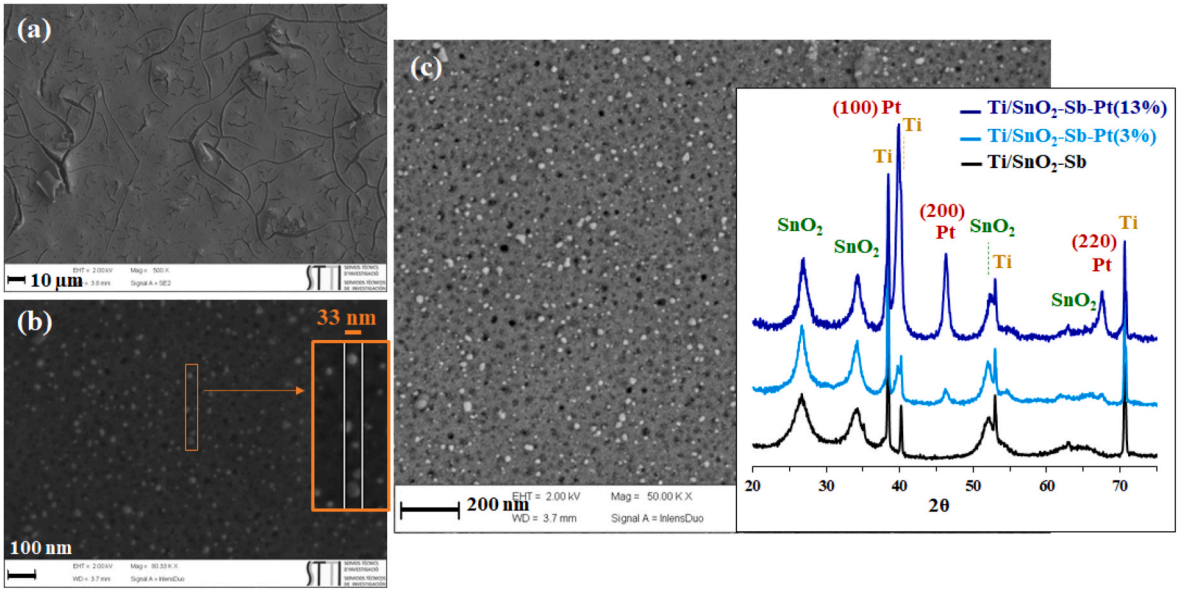

Fig. 1. FE-SEM images of the Ti/SnO_2–Sb–Pt (13%) anode: **(a)** 500 X, secondary electrons; **(B)** 80.33K X, secondary electrons; **(c)** 50K X, back-scattered electrons; Inset: X-ray diffractograms of the distinct Ti/SnO_2–Sb electrodes with variable Pt content.

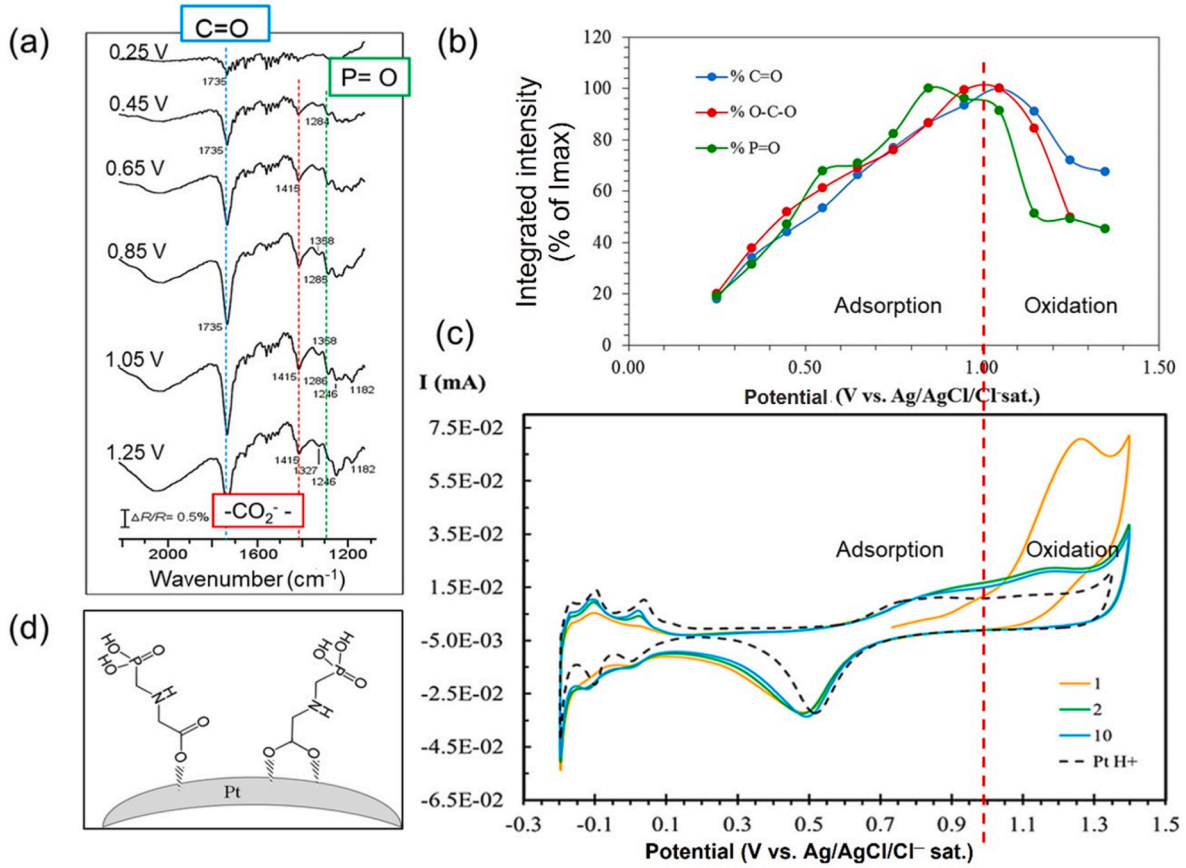

Fig. 2. **(a)** IR spectra of Poly-Pt electrode in the presence of GLP at different potentials. **(b)** Integration of the band intensity shown in (a) as a function of the applied potential. **(c)** Successive cyclic voltammograms of a Poly-Pt electrode in 200 mg L^{-1} GLP + 0.5 M H_2SO_4 aqueous solution with a scan rate of 50 mV s^{-1}. **(d)** Adsorption scheme proposed for the interaction of Pt and GLP.

related to Pt surface oxidation to PtOx, whereas the high intensity reduction peak centered at 0.51 V corresponds to the inverse process. Finally, the increasing anodic current above 1.30 V is attributed to the irreversible oxidation of water with oxygen evolution reaction (OER). When the electrode is submitted to potential cycling in presence of GLP (colored solid lines), a noticeable rising of anodic current appears during the first scan from 0.70 to 1.35 V. Particularly, the current raise becomes more marked from ca. 1.05 V, defining an oxidation peak centered at 1.27 V. This current peak is assigned to GLP oxidation process. Then, the oxidation current decreases in the subsequent cycles, probably due of a partial blockage of the electrode surface by oxidation by-products.

Interestingly, the obtained voltammetric response of GLP well complements the above-described in-situ IR results. On the one hand, the gradual increase of the three IR bands strongly suggests that GLP progressively adsorbs on the Pt surface at increasing electrode potential up to 1.00 V. Furthermore, the adsorption seems to occur mainly through the carboxylic group of GLP, in either the unidentate and/or the bidentate forms, as schematically proposed in Fig. 2d. This specific adsorption/interaction on Pt surface through carboxylate groups has been well reported in literature for other molecules (Huerta et al., 1997; Montilla et al., 2003; Zinola et al., 2005). On the other hand, the anodic peak together with the decay of IR-bands intensity indicates that GLP oxidizes on the surface of Pt above 1.00 V. Moreover, a new negative band at ca. 2340 cm^{-1} was found and developed above this potential (Fig. not shown). This band evidences the formation of CO_2 in solution nearest the electrode surface concurrently with GLP oxidation. Hence, these results clearly reflect the good capability of Pt to interact, oxidize and even mineralize GLP, thus, justifying its interest to be used as an electrocatalyst dopant in metal oxide electrodes for GLP oxidation.

3.3. Electrochemical behavior of Ti/SnO_2–Sb electrodes towards GLP oxidation

Fig. 3 shows the voltammetric response of the studied SnO_2–Sb electrodes overlapping the stationary response obtained in the sulfuric acid (dash line) with several cycles in presence of GLP (colored solid lines) (the response of the commercial Ti/Pt approaches that of Fig. 2c, while that of Si/BDD is included in Fig. S4). In absence of GLP, the voltammograms obtained for the three electrodes agree with those previously reported in the literature (Berenguer et al., 2009; Montilla et al., 2004a). When the platinum-free Ti/SnO_2–Sb electrode is submitted to successive potential cycles in presence of GLP (Fig. 3a), neither oxidation peaks nor significant voltammetric changes are discerned, at least in the region prior to the OER.

On the contrary, when a certain amount of Pt is introduced as a dopant (3% and 13% as shown in Fig. 3b and c, respectively), a rising oxidation current can be observed during the first cycle at potentials above 0.8 V, reaching a maximum at 1.1–1.2 V. This oxidation current decreases in the subsequent cycles, but it is still clearly observable above the response of the blank voltammogram (without GLP) in the case of the electrode with 13 % Pt. The similarity of these electrochemical features with those observed for Poly-Pt in Fig. 2c, and the fact that the oxidation current increases with the Pt content in the Ti/SnO_2–Sb electrode (Fig. 3), infer that the observed oxidative process corresponds to the electroxidation of GLP and/or by-products over Pt nanophases dispersed in Ti/SnO_2–Sb. In this sense, and although in-situ FT-IRRAS analysis cannot be performed on non-reflective SnO_2–Sb–Pt electrodes, from the polycrystalline structure of nano-sized Pt phases observed by XRD (inset of Fig. 1), and the clear Pt/PtOx oxidation and reduction

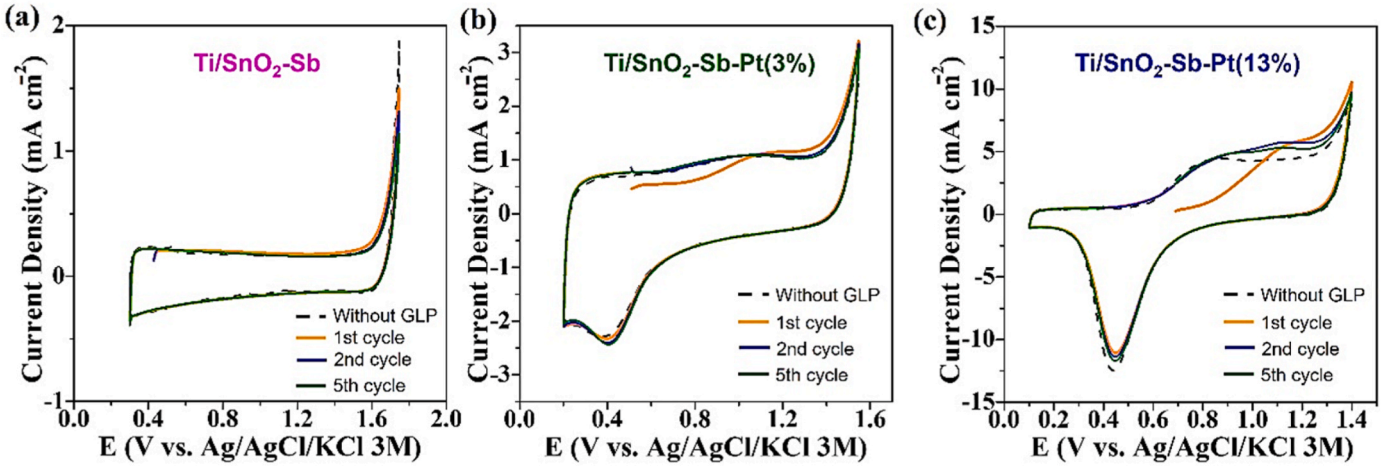

Fig. 3. Successive cyclic voltammograms of (a) Ti/SnO_2–Sb, (b) Ti/SnO_2–Sb–Pt (3%) and (c) Ti/SnO_2–Sb–Pt (13%) electrodes in a 0.5 M H_2SO_4 aqueous solution in absence or presence of 200 mg L^{-1} GLP. Scan rate = 50 mV s^{-1}.

irreversible features observed in the voltammograms, characteristic of polycrystalline Pt (Fig. 2c), it is quite reasonable and probable that the carboxylic-mediated GLP-Pt interaction observed on pure polycrystalline Pt (Fig. 2) may also occur on the Pt nanoparticles of the SnO_2–Sb–Pt electrodes. Hence, these voltammetric results suggest that the incorporation of small quantities of Pt as a dopant on Ti/SnO_2–Sb electrodes leads to an enhancement of their interaction with GLP and an improved GLP oxidative response (at least at potentials before the OER).

3.4. Electrolysis of GLP

Fig. 4 shows the evolution of phosphate concentration and TOC during the galvanostatic experiments with the self-prepared and commercial GLP solutions, whereas Table 1 collects different parameters calculated to evaluate the performance in the oxidation of GLP of each electrode. The dashed line in Fig. 4a represents the theoretical maximum phosphate concentration (112.3 mg L^{-1}) expected for a full conversion of GLP (200 mg L^{-1}) into phosphate (according to Eq. (1)). Among the results obtained for the prepared electrodes, a significative deactivation was observed for the Ti/SnO_2–Sb electrode at 5 h of treatment, thus impeding to continue the electrolysis from this point (see the electrode potentials in Table S1 and their evolution in Fig. S5 of SI). This effect did not appear on the rest of electrodes studied, thus corroborating the stabilization effect of Pt-doping expected on the Ti/SnO_2–Sb–Pt (x%) electrodes (Berenguer et al., 2014; Montilla et al., 2004a). Attending to the experimental results, the highest concentration of phosphate after 48 h of treatment, denoting the highest oxidation of GLP, was obtained for the commercial BDD electrode (ca. 100 % OE), followed by Ti/SnO_2–Sb–Pt (13%), Ti/SnO_2–Sb–Pt (3%) and finally the Ti/Pt electrode showing the worst performance (with 62, 53 and 20 % OE, respectively).

Fig. 4b shows the TOC evolution during these experiments. The dashed line depicts the theoretical value calculated for corresponding TOC to 200 mg L^{-1} of GLP, being 42.59 mg L^{-1}. The decreasing TOC is indicative of the capability of each electrode towards the mineralization of GLP and oxidation by-products. At the end of the treatment, the commercial Si/BDD electrode is the one which obtained the lowest TOC concentration (TE = 72 % at 48 h), followed again by Ti/SnO_2–Sb–Pt (13%) (TE = 52 %). The Ti/SnO_2–Sb–Pt (3%) and Ti/Pt electrodes, however, showed again a poorer performance, which was even more significant than in the case of GLP oxidation.

Fig. 4a and b also reflect that, independently of the anode, long times are required to oxidize and mineralize GLP. In fact, the additional x-axes at the top of the figures show the large charges needed to degrade this pollutant and the current efficiencies estimated for GLP mineralization (Eq. (5)) were found below 1 % for all the electrodes. These results emphasize the refractory character of GLP and/or its oxidation by-products. However, it is noteworthy to stress again that neither the optimization of reactor operation nor the optimization of electrochemical conditions for GLP oxidation have been the focus of this work. In this respect, several studies in the past have already demonstrated that efficiencies of electrochemical treatments can be remarkably enhanced by a suitable optimization of the different parameters.

On the other hand, the capability of the anodes to degrade GLP in a more real (complex) matrix was evaluated. Fig. 4c and d show the evolution of phosphate concentration and TOC, respectively, during the galvanostatic treatment of the commercial GLP product. Unlike the previous case, however, the unknown content of additives included in the commercial solution prevented us to determine a theoretical value of phosphate or TOC. As observed, the electrodes performance follows a similar trend to the case of self-prepared GLP solution (Fig. 4a and b). The Si/BDD anode reached higher phosphate concentration, COD removal (COD, E = 99 (%)) and mineralization (TE = 92 %), thus, being the most efficient electrode for degrading the commercial GLP. While Ti/SnO_2–Sb rapidly deactivated (after 2 h), the Ti/SnO_2–Sb–Pt (13%) electrode was also found to be stable and effective to oxidize and mineralize the commercial product. Interestingly, since it operates at considerably lower potentials (i.e. voltages) than Si/BDD (see SI), the Ti/SnO_2–Sb–Pt (13%) electrode is able to decrease TOC by consuming half energy (see U_{TOC} in Table 1). Finally, the Ti/SnO_2–Sb–Pt (3%) and Ti/Pt electrodes comparatively showed the poorest performances, although in this case the Ti/Pt electrode was found to produce a higher phosphate concentration.

3.4.1. Study of the GLP anodic oxidation reaction: evolution of by-products and pathways

Several samples were taken and analyzed by IC during the electrolytic experiments of the self-prepared solution to study GLP anodic oxidation reaction. Fig. 5 shows the evolution of GLP concentration, together with that of AMPA and PO_4^{3-} main by-products, while Table 2 summarizes the final concentration of these compounds and that of the analyzed organic anions and N-containing species (NO_3^-, NO_2^- and NH_4^+).

For Si/BDD (Fig. 5a), results show a total and fast conversion of GLP into AMPA and phosphate during the first 2 h, completing the total oxidation of AMPA after 5 h treatment. On the other hand, the oxidative treatment with this electrode results in the highest values of ammonium and nitrate as final products, and practically a negligible quantity of nitrite (Table 2). In this sense, the non-selective oxidizing capability of this electrode, favoring the production of nitrate, i.e., the most oxidized by-products, is probably a disadvantage of this electrode. Furthermore, Si/BDD finally cumulates the highest values of acetic and formic acids

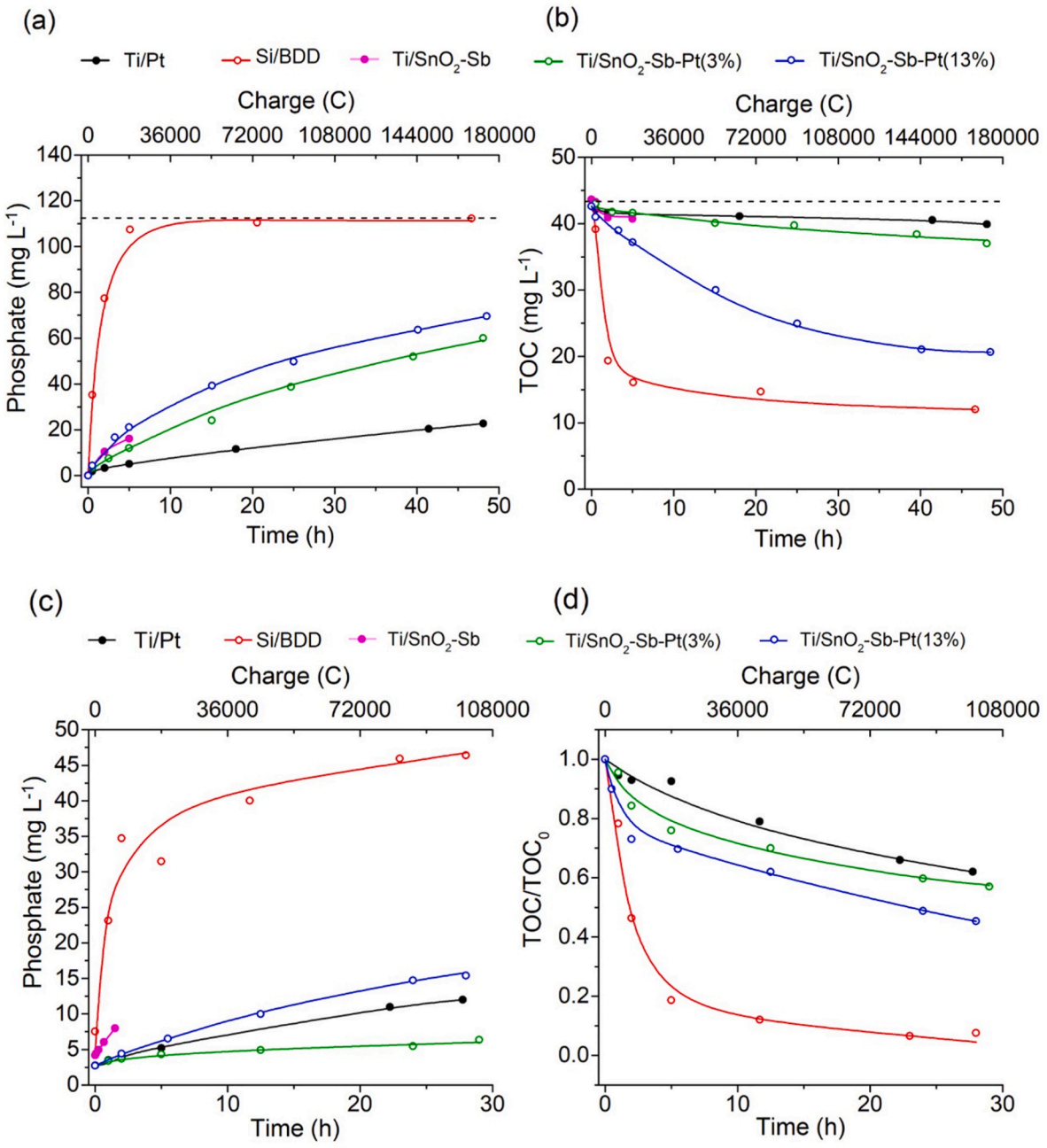

Fig. 4. Evolution of (a) phosphate concentration and (b) TOC during GLP electrolysis for the self-prepared GLP solution (200 mg L^{-1} GLP in a 0.5 M H_2SO_4). Evolution of (c) phosphate concentration and (d) normalized TOC during GLP electrolysis for the commercial GLP solution. Current density = 50 mA cm^{-2}.

Table 1
Parameters obtained from the electrolysis of GLP for each electrode studied.

Self-prepared GLP solution			
Electrode	**10^{-6} k_1 (s^{-1})**	**OE (%)**	**TE (%)**
Ti/Pt	1.23	20.2	6.4
Si/BDD	80.7	99.9	72.5
Ti/SnO_2–Sb	8.25[a]	14.4[a]	6.7[a]
Ti/SnO_2–Sb–Pt (3%)	4.26	53.4	13.2
Ti/SnO_2–Sb–Pt (13%)	4.29	61.9	51.6
Commercial GLP solution			
Electrode	**COD, E (%)**	**TE (%)**	**U_{TOC} (kJ L mg^{-1})**
Ti/Pt	22.1	38.0	13.1
Si/BDD	99.1	92.4	10.2
Ti/SnO_2–Sb–Pt (3%)	18.3	43.0	9.4
Ti/SnO_2–Sb–Pt (13%)	36.1	54.7	6.0

[a] Obtained at the time when electrode deactivated.

(see Table 2 and Fig. S6 in SI). This must be attributed not only to the higher performance to degrade GLP and AMPA, but also to the lower efficiency of this anode to oxidize C1 and C2 carboxylic acids at the high potentials reached during the electrolytic experiments (see Table S1) (Kapałka et al., 2008). From the found compounds, the reaction pathway for the anodic oxidation of GLP is proposed in the scheme of Fig. 5e. Please note that, although not quantified, the presence of oxalic acid was confirmed by CI too; and that the formation of other potential by-products, such as glycolic and glyoxylic acids, methanol or methyl amine, shouldn't be ruled out.

On the contrary, in the case of Ti/Pt (Fig. 5b) GLP is slowly oxidized to AMPA, which progressively accumulates up to 17 mg L^{-1} after 48 h, but the GLP concentration cannot be reduced below 135 mg L^{-1}. In parallel, the phosphate concentration slightly increases during the experiment, and formic acid, nitrate and ammonium are also detected,

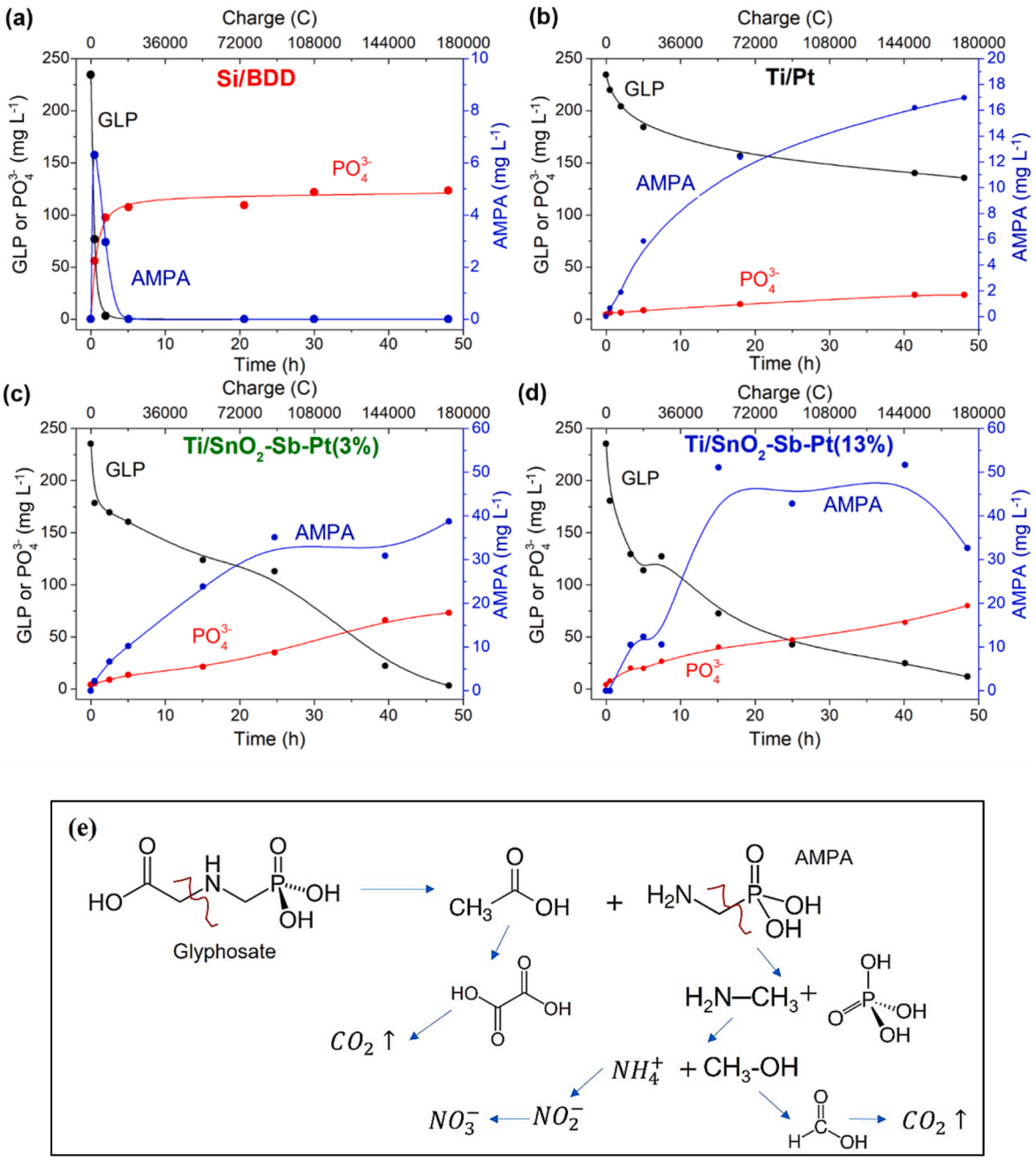

Fig. 5. Evolution of GLP concentration and that of its main oxidation by-products, determined by ionic chromatography, during the galvanostatic treatment of a self-prepared solution (200 mg L^{-1} GLP in a 0.5 M H_2SO_4) at 50 mA cm^{-2}, by using (a) Si/BDD, (b) Ti/Pt, (c) Ti/SnO_2–Sb–Pt (3%) and (d) Ti/SnO_2–Sb–Pt (13%) electrodes. (e) Proposed reaction scheme for the anodic oxidation of GLP with the studied anodes.

Table 2
Concentration of GLP and GLP oxidation by-products after 48 h of galvanostatic treatment (at 50 mA cm^{-2} of a self-prepared 200 mg L^{-1} GLP in a 0.05 M H_2SO_4 solution) measured by ionic chromatography.

Electrode	GLP mg L^{-1}	AMPA mg L^{-1}	PO_4^{3-} mg L^{-1}	Acetic mg L^{-1}	Formic mg L^{-1}	NO_2^- mg L^{-1}	NO_3^- mg L^{-1}	NH_4^+ mg L^{-1}
Ti/Pt	135.6	17.0	23.2	0.8	6.3	0.5	10.2	3.6
Si/BDD	0.0	0.0	123.3	29.7	8.6	0.4	38.6	13.7
Ti/SnO_2–Sb–Pt (3%)	3.1	38.7	73.4	2.4	5.2	0.3	7.8	7.0
Ti/SnO_2–Sb–Pt (13%)	5.5	32.76	80.1	0.0	5.2	0.4	17.8	2.6

in agreement with the scheme of Fig. 5e. These results indicate that this commercial electrode is considerably less efficient to oxidize GLP and AMPA.

The Pt-doped Ti/SnO_2–Sb electrodes (Fig. 5c and d) show considerably better response than Ti/Pt, but they cannot reach the oxidizing power of Si/BDD. Thus, both electrodes can oxidize almost the total amount of GLP, and they are effective to oxidize AMPA too, as deduced from the high phosphate production. Nevertheless, GLP

oxidation and AMPA generation are faster for the Ti/SnO_2–Sb–Pt (13%) (Fig. 5d). Furthermore, while for this electrode the AMPA concentration starts to decrease after reaching a maximum value, within the 20–30 h of treatment, it continuously increases for the Ti/SnO_2–Sb–Pt (3%) anode (Fig. 5c). Such a higher electrocatalytic activity exhibited by the electrode with higher Pt content is in agreement with the larger phosphate and nitrate concentrations found for the solutions treated with Ti/SnO_2–Sb–Pt (13%) (Table 2), the promoted generation of acetic and formic acids (see Fig. S6), as well as the measurements shown in Fig. 4a and b. In addition, this electrode exhibits a remarkably superior response to eliminate both acetic and formic acids (see Fig. S6), thus, justifying the observed low concentrations of these compounds at the end of the experiments (Table 2).

From these results it is found that the anodic oxidation of GLP proceeds through the formation of AMPA, becoming even more difficult to oxidize than GLP. This fact is clearly evidenced by the progressive accumulation of AMPA (Fig. 5) and may explain the low-medium TOC removal efficiencies observed for the different electrodes, except the case of Si/BDD (Table 1). The Si/BDD anode, however, can rapidly and completely oxidize both GLP and AMPA, but its limited capability to mineralize small carboxylic acids (Table 2) seems to justify why it is not capable to reach a TOC removal efficiency above 75 % (Table 1).

3.5. Electrocatalytic behavior of Pt-doped SnO_2–Sb electrodes

The long times needed to achieve GLP oxidation and TOC removal observed in Figs. 4 and 5 clearly reflect the refractory nature of GLP. Nonetheless, the better performance of Si/BDD is assigned to its greater capability for •OHs generation as well as their higher reactivity (since they are produced at much higher electrode potentials, ca. 6.0 V, see Table S1 in SI)), what makes GLP oxidation ca. 20 times faster than the other electrodes (from the comparison of k_1 values, Table 1).

By contrast, the obtained results indicate that, under the studied electrolytic conditions, the Ti/Pt and Ti/SnO_2–Sb anodes without enough Pt content (Ti/SnO_2–Sb–Pt (3%)) show poorer efficiency for GLP abatement. This suggests that the individual electrocatalytic features, mainly based on specific interactions for Pt or •OHs generation for the SnO_2-based material, may not be enough effective themselves. In this sense, the effect of Pt on the capability of SnO_2–Sb anodes towards •OHs generation was previously studied by using N,N-dimethyl-pnitrosoaniline (RNO), as radical scavenger, and monitored by in-situ UV spectroelectrochemical measurements (Fernández-Aguirre et al., 2020). This research demonstrated that the increase in Pt content from 3 to 13% slightly reduces the capability of the electrode towards •OHs generation, so a poorer electrocatalytic activity for GLP oxidation should be expected for the Ti/SnO_2–Sb–Pt (13%)). However, the opposite result has been found in this work, in agreement with the better response of this electrode for the oxidation of diclofenac (Fernández-Aguirre et al., 2020).

In order to explain the better performance observed for Ti/SnO_2–Sb–Pt (13%), it is proposed that the electrocatalytic effects observed for Pt (Fig. 2) and the •OHs generation capability in this SnO_2–Sb anode could synergistically cooperate for GLP oxidation. Thus, as schematically depicted in Fig. S7, the obtain results suggest that the Pt nanophases distributed on SnO_2–Sb (Fig. 1) may favor the adsorption of GLP (Figs. 2 and 3) near the sites in which the formation of •OHs is produced, promoting the subsequent GLP oxidation (Figs. 3–5). Pt is then proposed to destabilize and reduce the refractory character of GLP via metal-pollutant interactions, while the “non-active” nature of the SnO_2–Sb matrix must favor the generation of highly oxidizing (physisorbed) •OHs.

In the case of commercial Pt electrodes (Ti/Pt), these effects could be less efficient because of the “active” character of this electrode, promoting the generation of less-oxidizing (chemisorbed) •OHs and the OER (Cañizares et al., 2002; Martínez-Huitle and Ferro, 2006). This agrees with the lowest current efficiency and highest energy consumption found for this electrode (Table 1). Nevertheless, a too-strong adsorption of GLP and/or its by-products on Pt surface (as deduced from the current decay in the 2nd and 3rd voltammetric cycles, Fig. 2c) cannot be ruled out.

With respect to Pt-doped SnO_2–Sb electrodes, the comparatively lower activity shown by the Ti/SnO_2–Sb–Pt (3%) electrode, respect to that with 13%, may be explained by its lower catalyst content in the SnO_2–Sb matrix. In fact, it is well known that the electrocatalytic activity of Pt catalysts is very sensitive to many factors, highlighting defects and arrangement of Pt atoms; Pt crystalline planes; dimensions and morphology of Pt phases; dispersion and surface area, etc. (Shao et al., 2016; Vielstich et al., 2009). In this sense, although this work is uniquely devoted to demonstrating the promotion of GLP oxidation on Pt-doped SnO_2–Sb electrodes, a systematic study on the effect of the amount and size of Pt on the response of SnO_2-based electrodes is very interesting and deserves further research.

On the other hand, apart from Pt features, the nature and molecular structure of the pollutant may also be essential in this electrocatalytic mechanism. This work demonstrates that GLP adsorbs on Pt through its carboxylic group (Fig. 2), so this organic moiety must play a crucial role. In fact, this work also reveals an improved electrocatalytic response of Ti/SnO_2–Sb–Pt (13%)) towards the oxidation of two other carboxylic acids, like acetic and formic by-products (Fig. S6), and a similar behavior was found for diclofenac (Fernández-Aguirre et al., 2020), another carboxylic-containing emerging pollutant. Although further research would be needed to prove this, the potential extension of the synergistic oxidation mechanism of GLP induced by Pt and (•OHs) SnO_2–Sb to other carboxylic acids could have a major impact on anodic oxidation technology, since it is well known that the electrochemical oxidation of several organic molecules proceeds though the formation of carboxylic acids of different chain length.

4. Conclusions

The present research demonstrates the capability of Pt-doped SnO_2–Sb to oxidize and mineralize GLP herbicide, despite its marked refractory character, on either self-prepared or commercial solutions. Moreover, voltammetric and electrolytic experiments show that the electrocatalytic activity of the anodes towards GLP degradation increases with the Pt content in the range 0–13 met% in SnO_2–Sb anodes.

The good catalytic performance of these anodes has been attributed to their unique physicochemical properties. Thus, FE-SEM shows the segregation and uniform dispersion of Pt nanophases in the SnO_2–Sb matrix. The amount and size of these phases increase with the Pt content, displaying a diameter of less than 30 nm for the electrode with 13 met%. The combination of CV and in-situ FT-IRRAS measurements reveals the effective adsorption and subsequent oxidation of GLP on Pt surface. In particular, in situ FTIR spectroscopy indicates that GLP adsorption preferentially occurs through its carboxylic group. Interestingly, this specific interaction and oxidation of GLP on Pt has been voltammetrically observed also in the case of Pt-doped SnO_2–Sb electrodes. Considering that the introduction of Pt hinders •OHs generation on SnO_2–Sb electrodes (Fernández-Aguirre et al., 2020), it is proposed that the adsorption effects on Pt synergistically cooperate with the •OHs produced by the SnO_2–Sb matrix to electrocatalyze the GLP oxidation and mineralization.

Under the used but non-optimized experimental conditions, the comparison with commercial electrodes shows the superior performance of the Si/BDD anode towards the elimination of GLP and AMPA, the main oxidation by-products. By contrast, the Ti/Pt electrode has displayed the worst performance among the studied electrodes, and that of the studied Pt-doped SnO_2–Sb electrodes lie in between these commercial anodes. For Ti/SnO_2–Sb electrodes, the addition of Pt as a dopant is crucial to enhance stability, and remarkably affects their electrocatalytic activity. Thus, the obtained results demonstrate that the Ti/SnO_2–Sb–Pt (13%) electrode exhibits higher efficiencies and faster kinetics for GLP,

AMPA, DQO and TOC elimination than the electrode with 3 met% Pt and commercial Ti/Pt. Remarkably, this electrode can eliminate GLP by consuming half of the energy needed by the BDD electrode. This advantage together with the significant lower cost and higher mechanical stability of Pt-doped Ti/SnO_2–Sb anodes enable to propose them as cheaper alternatives to BDD for the elimination of glyphosate and derived herbicides in water.

Author contributions statement

R. Berenguer: Validation, Data curation, Writing – original draft, Visualization, Supervision, Writing-Reviewing and Editing, Funding acquisition. M. G. Fernández-Aguirre: Investigation. S. Beaumont: Investigation, Data curation, Writing – original draft. F. Huerta: Investigation, Methodology, Writing-Reviewing and Editing. E. Morallón: Conceptualization, Resources, Methodology, Writing-Reviewing and Editing, Project administration, Funding acquisition.

Declaration of competing interest

The authors declare that they have no known competing financial interests or personal relationships that could have appeared to influence the work reported in this paper.

Data availability

Data will be made available on request.

Acknowledgements

The authors gratefully acknowledge the EDGJID/2021/330 contract (Generalitat Valenciana, Spain), as well as the RYC-2017-23618 contract and TED2021-131028B–I00 project funded by MCIN/AEI/10.13039/501100011033 and “ESF Investing in your future” and “European Union NextGeneration EU/PRTR”.

Appendix A. Supplementary data

Supplementary data to this article can be found online at https://doi.org/10.1016/j.chemosphere.2023.140635.

References

Assalin, M.R., de Moraes, S.G., Queiroz, S.C.N., Ferracini, V.L., Duran, N., 2010. Studies on degradation of glyphosate by several oxidative chemical processes: ozonation, photolysis and heterogeneous photocatalysis. J. Environ. Sci. Health Part B Pestic. Food Contam. Agric. Wastes 45, 89–94.

Balci, B., Oturan, M.A., Oturan, N., Sires, I., 2009. Decontamination of aqueous glyphosate, (aminomethyl) phosphonic acid, and glufosinate solutions by electro-fenton-like process with Mn^{2+} as the catalyst. J. Agric. Food Chem. 57, 4888–4894, 2009.

Barrett, K.A., Mcbride, M.B., 2005. Oxidative Degradation of glyphosate and aminomethylphosphonate by manganese oxide. Environ. Sci. Technol. 39, 9223–9228.

Berenguer, R., Quijada, C., Morallón, E., 2009. Electrochemical characterization of SnO_2 electrodes doped with Ru and Pt. Electrochim. Acta 54, 5230–5238.

Berenguer, R., Sieben, J.M., Quijada, C., Morallón, E., 2014. Pt- and Ru-doped SnO_2-Sb anodes with high stability in alkaline medium. ACS Appl. Mater. Interfaces 6, 22778–22789.

Berenguer, R., Sieben, J.M., Quijada, C., Morallón, E., 2016. Electrocatalytic degradation of phenol on Pt- and Ru-doped Ti/SnO_2-Sb anodes in an alkaline medium. Appl. Catal. B Environ. 199, 394–404.

Berenguer, R., La Rosa-Toro, A., Quijada, C., Morallón, E., 2017. Electrocatalytic oxidation of cyanide on copper-doped cobalt oxide electrodes. Appl. Catal. B Environ. 207, 286–296.

Berenguer, R., La Rosa-Toro, A., Quijada, C., Morallón, E., 2019a. Electro-oxidation of CN on active and non-active anodes. Designing the electrocatalytic response of cobalt spinels. Sep. Purif. Technol. 208, 42–50.

Berenguer, R., Quijada, C., Morallón, E., 2019b. The nature of the electro-oxidative catalytic response of mixed metal oxides: Pt- and Ru-doped SnO_2 anodes. Chemelectrochem 6 (4), 1057–1068.

Cañizares, P., Martínez, F., Díaz, M., García-Gómez, J., Rodrigo, M.A., 2002. Electrochemical oxidation of aqueous phenol wastes using active and nonactive electrodes. J. Electrochem. Soc. 149, D118–D124.

Carneiro, R.T.A., Taketa, T.B., Gomes Neto, R.J., Oliveira, J.L., Campos, E.V.R., de Moraes, M.A., da Silva, C.M.G., Beppu, M.M., Fraceto, L.F., 2015. Removal of glyphosate herbicide from water using biopolymer membranes. J. Environ. Manag. 151, 353–360.

Comninellis, Ch, Pulgarin, C., 1993. Electrochemical oxidation of phenol for wastewater treatment using SnO_2 anodes. J. Appl. Electrochem. 23, 108–112.

Deblonde, T., Cossu-Leguille, C., Hartemann, P., 2011. Emerging pollutants in wastewater: a review of the literature. Int. J. Hyg Environ. Health 214, 442, 2011.

De Santana, H., Toni, L.R.M., Benetoli, L.O.B., Zaia, C.T.B.V., Rosa Jr., M., Zaia, D.A.M., 2006. Effect in glyphosate adsorption on clays and soils heated and characterization by FT-IR spectroscopy. Geoderma 136, 738–750.

De Souza, D.R., Trovõ, A.G., Antoniosi Filho, N.R., Silva, M.A.A., Machado, A.E.H., 2013. Degradation of the commercial herbicide glyphosate by photo-fenton process: evaluation of kinetic parameters and toxicity. J. Braz. Chem. Soc. 24 (9), 1451–1460.

European Commission, 2023. Glyphosate. https://ec.europa.eu/food/plants/pesticides/approval-active-substances/renewal-approval/glyphosate_en.

Fernández-Aguirre, M.G., Berenguer, R., Beaumont, S., Nuez, M., La Rosa-Toro, A., Peralta-Hernández, J.M., Morallón, E., 2020. The generation of hydroxyl radicals and electro-oxidation of diclofenac on Pt-doped SnO_2-Sb electrodes. Electrochim. Acta 354, 136686.

Geissen, V., Mol, H., Klumpp, E., Umlauf, G., Nadal, M., Van Der Ploeg, M., Van De Zee, S.E.A.T.M., Ritsema, C.J., 2015. Emerging pollutants in the environment: a challenge for water resource management. Int. Soil Water Conserv. Res. 3, 57–65.

Glass, R.L., 1987. Adsorption of glyphosate by soils and clay minerals. J. Agric. Food Chem. 35, 497–500.

Grosse, Y., Loomis, D., Guyton, K.Z., El Ghissassi, F., Bouvard, V., Benbrahim-Tallaa, L., Mattock, H., Straif, K., 2016. Carcinogenicity of some industrial chemicals. Lancet Oncol. 17, 419–420.

Heinrich, K.F.J., 1968. Quantitative Electron Probe Microanalysis. National Bureau of Standards Special Publication, vol. 298. U.S. Department of Commerce/U.S. Government Printing Office, Washington D.C.

Hosseini, N., Toosi, M.R., 2019. Removal of 2,4-D, glyphosate, trifluralin, and butachlor herbicides from water by polysulfone membranes mixed by graphene oxide/TiO_2 nanocomposite: study of filtration and batch adsorption. J. Environ. Heal. Sci. Eng. 17, 247–258.

Huerta, F., Morallón, E., Cases, F., Rodes, A., Vázquez, J.L., Aldaz, A., 1997. Electrochemical behaviour of amino acids on Pt(h,k,l): a voltammetric and in situ FTIR study. Part 1. Glycine on Pt(111). J. Electroanal. Chem. 421, 179–185.

Ikehata, K., El-Din, M.G., 2006. Aqueous pesticide degradation by hydrogen peroxide/ultraviolet irradiation and Fenton-type advanced oxidation processes: a review. J. Environ. Eng. Sci. 5, 81–135.

IndustryARC, 2022. Glyphosate Market – Forecast (2023-2028), Hyderabad, India. https://www.industryarc.com/Research/Glyphosate-Market-Research-503411.

International Service for the Acquisition of Agri-biotech Applications (ISAAA), 2020. Herbicide Tolerance Technology: Glyphosate and Glufosinate. https://www.isaaa.org/resources/publications/pocketk/10/default.asp.

Iwasita, T., Nart, F.C., 1995. In-situ Fourier transform infrared spectroscopy: a tool to characterize the metal-electrolyte interface at a molecular level. In: Gerischer, H., Tobias, C.W. (Eds.), Advances in Electrochemical Science and Engineering. Wiley-VCH, Weinheim, pp. 123–216.

Kalofiri, P., Balias, G., Tekos, F., 2021. The EU endocrine disruptors' regulation and the glyphosate controversy. Toxicol Rep 8, 1193–1199.

Kapałka, A., Fóti, G., Comninellis, Ch, 2008. Investigation of the anodic oxidation of acetic acid on boron-doped diamond electrodes. J. Electrochem. Soc. 155, E27–E32.

Kapałka, A., Fóti, G., Comninellis, Ch, 2009. The importance of electrode material in environmental electrochemistry. Formation and reactivity of free hydroxyl radicals on boron-doped diamond electrodes. Electrochim. Acta 54, 2018–2023.

Kapałka, A., Fóti, G., Comninellis, Ch, 2010. Basic principles of the electrochemical mineralization of organic pollutants for wastewater treatment. In: Comninellis, Ch, Chen, G. (Eds.), Electrochemistry for the Environment. Springer, New York, pp. 1–23.

Kissane, Z., Shephard, J.M., 2017. The rise of glyphosate and new opportunities for biosentinel early-warning studies. Conserv. Biol. 31, 1293–1300.

Klug, H.P., Alexander, L.E., 1974. X-Ray Diffraction Procedures: for Polycrystalline and Amorphous Materials, second ed. Wiley-VCH, Weinheim.

Konishi, T., Kiguchi, M., Murakoshi, K., 2007. Quantized conductance behavior of Pt metal nanoconstrictions under electrochemical potential control. Surf. Sci. 601, 4122–4126.

Kukurina, O., Elemesova, Z., Syskina, A., 2014. Mineralization of organophosphorous pesticides by electro-generated oxidants. Procedia Chem. 10, 209–216.

Lamastra, L., Balderacchi, M., Trevisan, M., 2016. Inclusion of emerging organic contaminants in groundwater monitoring plans. MethodsX 3, 459–476.

Lan, Y., Coetsier, C., Causserand, C., Groenen Serrano, K., 2018. An experimental and modelling study of the electrochemical oxidation of pharmaceuticals using a boron-doped diamond anode. Chem. Eng. J. 333, 486–494.

Loos, G., Scheers, T., Van Eyck, K., Van Schepdael, A., Adams, E., Van der Bruggen, B., Cabooter, D., Dewil, R., 2018. Electrochemical oxidation of key pharmaceuticals using a boron doped diamond electrode. Sep. Purif. Technol. 195, 184–191.

Lozeman, J.J.A., Führer, P., Olthuis, W., Odijk, M., 2020. Spectroelectrochemistry, the future of visualizing electrode processes by hyphenating electrochemistry with spectroscopic techniques. Analyst 145, 2482–2509.

Mañas, F., Peralta, L., Raviolo, J., García-Ovando, H., Weyers, A., Ugnia, L., Gonzalez-Cid, M., Larripa, I., Gorla, N., 2009. Genotoxicity of AMPA, the environmental

metabolite of glyphosate, assessed by the Comet assay and cytogenetic tests. Ecotoxicol. Environ. Saf. 72, 834–837.
Mariani, M.L., Romero, R.L., Zalazar, C.S., 2015. Modeling of degradation kinetic and toxicity evaluation of herbicides mixtures in water using the UV/H_2O_2 process. Photochem. Photobiol. Sci. 14, 608–617.
Marselli, B., García-Gómez, J., Michaud, P.-A., Rodrigo, M.A., Comninellis, Ch, 2003. Electrogeneration of hydroxyl radicals on boron-doped diamond electrodes. J. Electrochem. Soc. 150, D79–D83.
Martínez-Huitle, C.A., Ferro, S., 2006. Electrochemical oxidation of organic pollutants for the wastewater treatment: direct and indirect processes. Chem. Soc. Rev. 35, 1324–1340.
Montenegro-Ayo, R., Pérez, T., Lanza, M.R.V., Brillas, E., Garcia-Segura, S., dos Santos, A.J., 2023. New electrochemical reactor design for emergent pollutants removal by electrochemical oxidation. Electrochim. Acta 458, 142551.
Montilla, F., Morallón, E., Vázquez, J.L., 2003. Electrochemical behaviour of benzoic acid on platinum and gold electrodes. Langmuir 19, 10241–10246.
Montilla, F., Morallón, E., De Battisti, A., Vázquez, J.L., 2004a. Preparation and characterization of antimony-doped tin dioxide electrodes. Part 1. Electrochemical characterization. J. Phys. Chem. B 108, 5036–5043.
Montilla, F., Morallón, E., De Battisti, A., Benedetti, A., Yamashita, H., Vázquez, J.L., 2004b. Preparation and characterization of antimony-doped tin dioxide electrodes. Part 2. XRD and EXAFS characterization. J. Phys. Chem. B 104, 5044–5050.
Montilla, F., Morallón, E., De Battisti, A., Barison, S., Daolio, S., Vázquez, J.L., 2004c. Preparation and characterization of antimony-doped tin dioxide electrodes. 3. XPS and SIMS characterization. J. Phys. Chem. B 108, 15976–15981.
Montilla, F., Morallón, E., A, Vázquez, J.L., 2005. Evaluation of the electrocatalytic activity of antimony-doped tin dioxide anodes toward the oxidation of phenol in aqueous solutions. J. Electrochem. Soc. 152, B421–B427.
Mordor Intelligence, 2022. Glyphosate Market Size & Share Analysis-Growth Trends & Forecasts (2023-2028. Hyderabad, India. https://www.mordorintelligence.com/industry-reports/glyphosate-herbicide-market.
Morillo, E., Undabeytia, T., Maqueda, C., 1997. Adsorption of glyphosate on the clay mineral montmorillonite: effect of Cu(II) in solution and adsorbed on the mineral. Environ. Sci. Technol. 31, 3588–3592.
Muneer, M., Boxall, C., 2008. Photocatalyzed degradation of a pesticide derivative glyphosate in aqueous suspensions of titanium dioxide. Int. J. Photoenergy 2008, 197346.
Neto, S.A., de Andrade, A.R., 2009. Electrooxidation of glyphosate herbicide at different DSA® compositions: pH, concentration and supporting electrolyte effect. Electrochim. Acta 54, 2039–2045.
Nourouzi, M.M., Chuah, T.G., Choong, T.S.Y., 2010. Adsorption of glyphosate onto activated carbon derived from waste newspaper. Desalination Water Treat. 24, 321–326.
Oláh, M., Farkas, E., Székács, I., Horvath, R., Székács, A., 2022. Cytotoxic effects of Roundup Classic and its components on NE-4C and MC3T3-E1 cell lines determined by biochemical and flow cytometric assays. Toxicol Rep 9, 914–926.
Panizza, M., Michaud, P.A., Cerisola, G., Comninellis, Ch, 2001. Anodic oxidation of 2-naphthol at boron-doped diamond electrodes. J. Electroanal. Chem. 507, 206–214.
Panizza, M., Cerisola, G., 2009. Direct and mediated anodic oxidation of organic pollutants. Chem. Rev. 109 (12), 6541–6569.
Polcaro, A.M., Palmas, S., Renoldi, F., Mascia, M., 1999. On the performance of Ti/SnO_2 and Ti/PbO_2 anodes in electrochemical degradation of 2-chlorophenol for wastewater treatment. J. Appl. Electrochem. 29, 147–151.
Rodrigo, M.A., Michaud, P.A., Duo, I., Panizza, M., Cerisola, G., Comninellis, Ch, 2001. Oxidation of 4-chlorophenol at boron-doped diamond electrode for wastewater treatment. J. Electrochem. Soc. 148, D60–D64.
Rubí-Juárez, H., Cotillas, S., Sáez, C., Cañizares, P., Barrera-Díaz, C., Rodrigo, M.A., 2016. Removal of herbicide glyphosate by conductive-diamond electrochemical oxidation. Appl. Catal. B Environ. 188, 305–312.
Shao, M., Chang, Q., Dodelet, J.P., Chenitz, R., 2016. Recent advances in electrocatalysts for oxygen reduction reaction. Chem. Rev. 116, 3594–3657.
Sirés, I., Brillas, E., 2012. Remediation of water pollution caused by pharmaceutical residues based on electrochemical separation and degradation technologies: a review. Environ. Int. 40, 212–229.
Socrates, G., 1994. Infrared Characteristic Group Frequencies. Wiley, New York.
Székács, A., Darvas, B., 2018. Re-registration challenges of glyphosate in the European Union. Front. Environ. Sci. 6, 78.
Tran, N., Drogui, P., Doan, T.L., Le, T.S., Nguyen, H.C., 2017. Electrochemical degradation and mineralization of glyphosate herbicide. Environ. Technol. 38, 2939–2948.
Transparency Market Research, 2022. Glyphosate Market - Global Industry Analaysis, Size, Share, Growth, Trends, and Forecast. Delaware, USA, pp. 2021–2031. https://www.transparencymarketresearch.com/glyphosate-market.html.
Trasatti, S., 2000. Electrocatalysis: understanding the success of DSA®. Electrochim. Acta 45 (15–16), 2377–2385.
Vielstich, W., Hubert, A., Gasteiger, H.A., Yokokawa, H., 2009. Volumes 5 and 6. In: Handbook of Fuel Cells: Advances in Electrocatalysis, Materials, Diagnostics and Durability. Wiley, Chichester.
Wang, J.L., Xu, L.J., 2012. Advanced oxidation processes for wastewater treatment: formation of hydroxyl radical and application. Crit. Rev. Environ. Sci. Technol. 42, 251–325.
World Health Organization, 2017. Some organophosphate insecticides and herbicides. IARC (Int. Agency Res. Cancer) Monogr. Eval. Carcinog. Risks Hum. 112.
Zhang, K., Deletic, A., Page, D., McCarthy, D.T., 2015. Surrogates for herbicide removal in stormwater biofilters. Water Res. 81, 64–71.
Zinola, C.F., Rodríguez, J.L., Arévalo, M.C., Pastor, E., 2005. FTIR studies of tyrosine oxidation at polycrystalline Pt and Pt(111) electrodes. J. Electroanal. Chem. 585, 230–239.